

GLI activation by atypical protein kinase C ι/λ regulates the growth of basal cell carcinomas

Scott X. Atwood¹, Mischa Li¹, Alex Lee¹, Jean Y. Tang¹ & Anthony E. Oro¹

Growth of basal cell carcinomas (BCCs) requires high levels of hedgehog (HH) signalling through the transcription factor GLI¹. Although inhibitors of membrane protein smoothed (SMO) effectively suppress HH signalling, early tumour resistance illustrates the need for additional downstream targets for therapy^{1–6}. Here we identify atypical protein kinase C ι/λ (aPKC- ι/λ) as a novel GLI regulator in mammals. aPKC- ι/λ and its polarity signalling partners⁷ co-localize at the centrosome and form a complex with missing-in-metastasis (MIM), a scaffolding protein that potentiates HH signalling^{8,9}. Genetic or pharmacological loss of aPKC- ι/λ function blocks HH signalling and proliferation of BCC cells. *Prkci* is a HH target gene that forms a positive feedback loop with GLI and exists at increased levels in BCCs. Genome-wide transcriptional profiling shows that aPKC- ι/λ and SMO control the expression of similar genes in tumour cells. aPKC- ι/λ functions downstream of SMO to phosphorylate and activate GLI1, resulting in maximal DNA binding and transcriptional activation. Activated aPKC- ι/λ is upregulated in SMO-inhibitor-resistant tumours and targeting aPKC- ι/λ suppresses signalling and growth of resistant BCC cell lines. These results demonstrate that aPKC- ι/λ is critical for HH-dependent processes and implicates aPKC- ι/λ as a new, tumour-selective therapeutic target for the treatment of SMO-inhibitor-resistant cancers.

To identify new druggable targets in the HH pathway, we used the scaffold protein MIM, which potentiates GLI-dependent activation downstream of SMO (ref. 9), as bait in a biased proteomics screen of factors involved in HH signalling and ciliogenesis. Two of the hits were polarity proteins not previously linked to the HH pathway: aPKC- ι/λ , a serine/threonine kinase, and PARD3, a scaffold protein and aPKC- ι/λ substrate (Supplementary Fig. 1a). Reciprocal immunoprecipitation of aPKC- ι/λ and PARD3 pulled down MIM, suggesting a specific interaction (Supplementary Fig. 1b). Because MIM is a centrosome-associated protein that promotes ciliogenesis⁸, we fractionated centrosomes and found that aPKC- ι/λ , along with PARD3 and PARD6A, co-fractionated and co-immunoprecipitated with MIM in γ -tubulin-positive fractions that mark centrosomes (Fig. 1a and Supplementary Fig. 1c). MIM partly co-localizes with aPKC- ι/λ -complex members at the basal body in dermal fibroblasts, keratinocytes and the well-characterized mouse BCC cell line ASZ001¹⁰ (Fig. 1b), where aPKC- ι/λ and MIM interact through co-immunoprecipitation (Fig. 1c). Loss of aPKC- ι/λ or MIM protein suppressed HH signalling, because messenger RNA (mRNA) levels of the HH target gene *Gli1* were reduced and ciliogenesis was inhibited (Fig. 1d, e and Supplementary Fig. 1d, e).

Because the kinase activity is necessary for many of the cellular functions of aPKC- ι/λ (refs 7, 11), we used a myristoylated aPKC

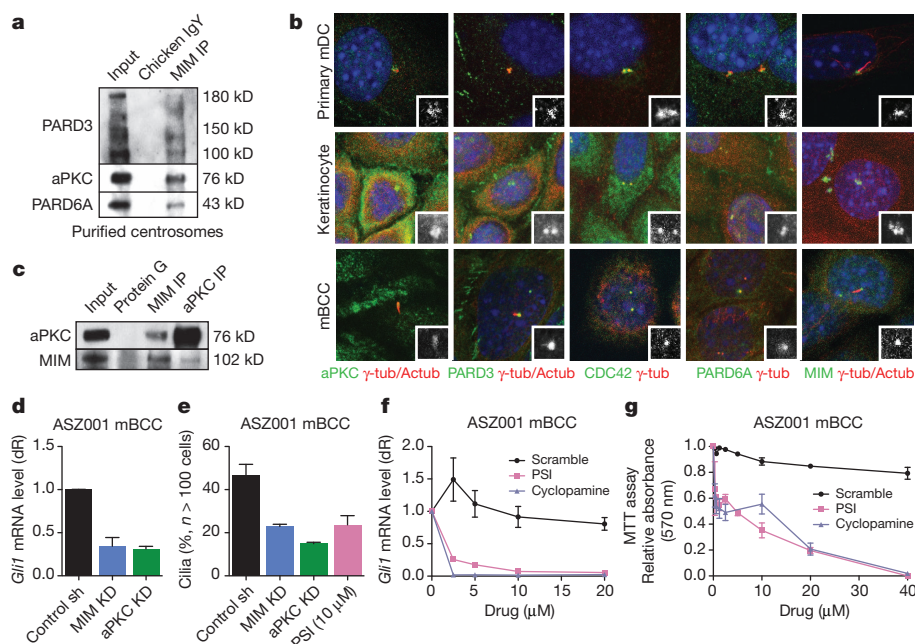


Figure 1 | aPKC- ι/λ is a centrosome-associated protein that regulates HH signalling. **a**, MIM and aPKC- ι/λ interact in purified centrosomes. IgY, immunoglobulin-Y. **b**, MIM and aPKC- ι/λ complexes localize at the centrosome (γ -tub, γ -tubulin) versus primary cilia (Actub, acetylated tubulin) of mouse dermal cells (mDC), mouse keratinocytes and mouse BCC cells (mBCC). **c**, MIM

and aPKC- ι/λ interact in BCC cells. **d–f**, *Gli1* mRNA levels ($n = 3$) or cilia percentage ($n = 3$) after *MIM* or aPKC- ι/λ short hairpin (sh) RNA knockdown, or aPKC or SMO inhibition in BCC cells. KD, knockdown. **g**, Cell proliferation was decreased in BCC cells ($n = 3$) after PSI or cyclopamine treatment, but not after treatment with myristoylated scrambled peptide. Error bars, s.e.m.

¹Program in Epithelial Biology, Stanford University School of Medicine, Stanford, California 94305, USA.

peptide inhibitor (PSI) to suppress kinase activity¹² (Supplementary Fig. 1f). PSI, but not a myristoylated scrambled peptide, inhibited HH signalling in BCC cells in a dose-dependent manner similar to the SMO antagonist cyclopamine (Fig. 1f). PSI, the pan-PKC inhibitor Go6983 and genetic loss of aPKC-1/ λ expression also resulted in dose-dependent inhibition of cell growth in BCC cells, leading to cell death according to MTT assay (Fig. 1g and Supplementary Fig. 1g, h). PSI inhibited BCC cell growth at a concentration similar to that of cyclopamine, with a half-maximal inhibitory concentration (IC₅₀) of 5 μ M. Primary cilia were reduced by 50% in PSI-treated BCC cells (Fig. 1e), indicating that aPKC activity is critical to both HH signalling and ciliogenesis in BCC cells. Interestingly, PSI did not affect proliferation in several non-tumorigenic cells (Supplementary Fig. 1i). PSI specifically inhibited aPKC, because loss of aPKC-1/ λ in BCC cells in combination with PSI treatment possessed no additional activity to reduce levels of *Gli1* or *Prkci* mRNA (Supplementary Fig. 1j).

To address whether the effects of aPKC-1/ λ on the HH pathway are direct, we assayed aPKC-1/ λ function in several nonpolar cell lines (Supplementary Fig. 1k, l and data not shown). These cells maintained their primary cilia or developed more after loss of aPKC-1/ λ ; however, aPKC-1/ λ removal still blocked HH activation, reducing target gene induction. We conclude that the effects of aPKC-1/ λ on HH signalling are cilia independent and are required for maximal sustained signalling.

aPKC-1/ λ is necessary for maximal HH signalling, and so we next investigated whether aPKC-1/ λ is overexpressed in BCCs. Indeed, *Prkci* expression, but not *Prkcz* expression, is specifically upregulated with *Gli1* in BCC cells (Fig. 2a). Similar results are found using freshly isolated human BCCs compared with primary human keratinocytes (Fig. 2b). Immunohistochemical staining of human BCCs and normal skin with antibodies recognizing both total and activated aPKC (P-aPKC) show higher levels in invasive and nodular tumours, with P-aPKC showing greater overexpression (Fig. 2c). Loss of aPKC-1/ λ removes both aPKC and P-aPKC staining in primary mouse dermal cells, indicating the specificity of the antibody (Supplementary Fig. 2).

Because aPKC-1/ λ and HH signalling are required for BCC cell growth, we then asked whether *Prkci* is a HH target gene. Activation of HH signalling in both polarized and non-polarized primary and immortalized cells using SHH-N ligand (the amino-terminal fragment of SHH) induces both *Gli1* and *Prkci* transcripts, but not *Prkcz* (Fig. 2d). Additionally, when we block HH signalling by treating BCC cells with cyclopamine, *Gli1* and *Prkci* transcripts, but not *Prkcz*, are specifically suppressed (Fig. 2g). Three putative GLI1-binding sites¹³ are present in the promoter region within 5 kilobases of the *Prkci* transcriptional start site in mice (Fig. 2e). Chromatin immunoprecipitation (ChIP) with BCC cells overexpressing FLAG:GLI1 enrich in regions containing the three GLI1-binding sites (Fig. 2f), indicating that *Prkci* is a direct target of GLI1. The first two GLI1-binding sites promote expression of luciferase when expressed in BCC cells, suggesting that these sites are functional (Supplementary Fig. 3). In addition, expression of *Pard6a* (aPKC-1/ λ inhibitor) is reduced whereas *Cdc42* (activator) is overexpressed in primary mouse BCC tumours¹⁴ (Fig. 2h). Because aPKC-1/ λ is typically found in an inhibited PARD6A complex, less PARD6A would result in excessive free and active aPKC-1/ λ whereas more CDC42 would activate any existing PARD6A-aPKC-1/ λ complexes. Interestingly, when HH signalling is inhibited with the SMO antagonist SANT-1, *Pard6a* transcript levels are increased and *Cdc42* levels are decreased (Fig. 2i), further supporting the idea that HH signalling promotes aPKC-1/ λ activation. We conclude that aPKC-1/ λ is part of a HH-mediated positive feedback loop leading to its overexpression in human and mouse BCCs.

To gain insight into aPKC-1/ λ 's mechanism of action, we determined whether aPKC-1/ λ -dependent genes in tumours differed from those regulated by SMO. We treated BCC cells with SANT-1 or PSI and performed 3'-end polyadenylated RNA sequencing. We found that the expression level of 5,700 SANT-1-dependent and 4,762

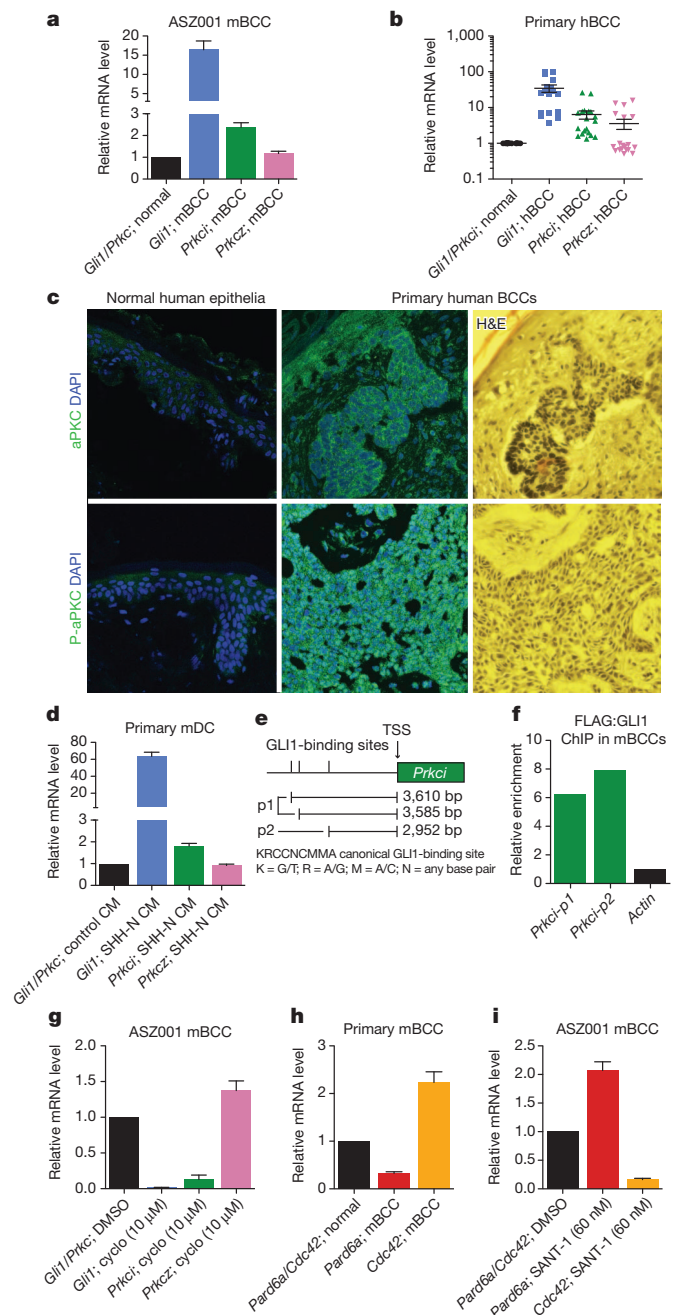


Figure 2 | aPKC-1/ λ and HH form a positive-feedback loop in BCCs.

a, **b**, *Gli1*, *Prkci*, and *Prkcz* mRNA levels in mouse BCC cells (**a**) ($n = 3$) and primary human BCC tumours (**b**; hBCC) ($n = 7$). **c**, Total and activated aPKC-1/ λ (P-aPKC) overexpressed in primary human BCC tumours. **d**, *Prkci* is upregulated in SHH-N-treated mouse dermal cells ($n = 3$). CM, conditioned media. **e**, GLI1-binding sites within the promoter region of *Prkci*. TSS, transcriptional start site. **f**, FLAG:GLI1 ChIP of *Prkci* promoter GLI1 sites. **g**, Cyclopamine suppresses *Prkci* expression in BCC cells ($n = 3$). **h**, *Pard6a* expression is reduced and *Cdc42* is upregulated in mouse BCC tumours ($n = 3$). **i**, SANT-1-treatment of BCC cells increases *Pard6a* and decreases *Cdc42* mRNA expression ($n = 3$). Error bars, s.e.m.

PSI-dependent transcripts changed twofold or more when compared with a control (Fig. 3a). Also, 4,325 transcripts overlapped between the inhibitor-treated data sets ($P < 1.0 \times 10^{-300}$), with most transcripts being downregulated in both sets (Fig. 3b). Gene ontology terms associated with commonly changed transcripts include cell cycle regulation, protein transport and localization, and cell division (Fig. 3c). Global transcript expression regardless of fold-change showed a strong positive correlation between drug treatments, with a Pearson

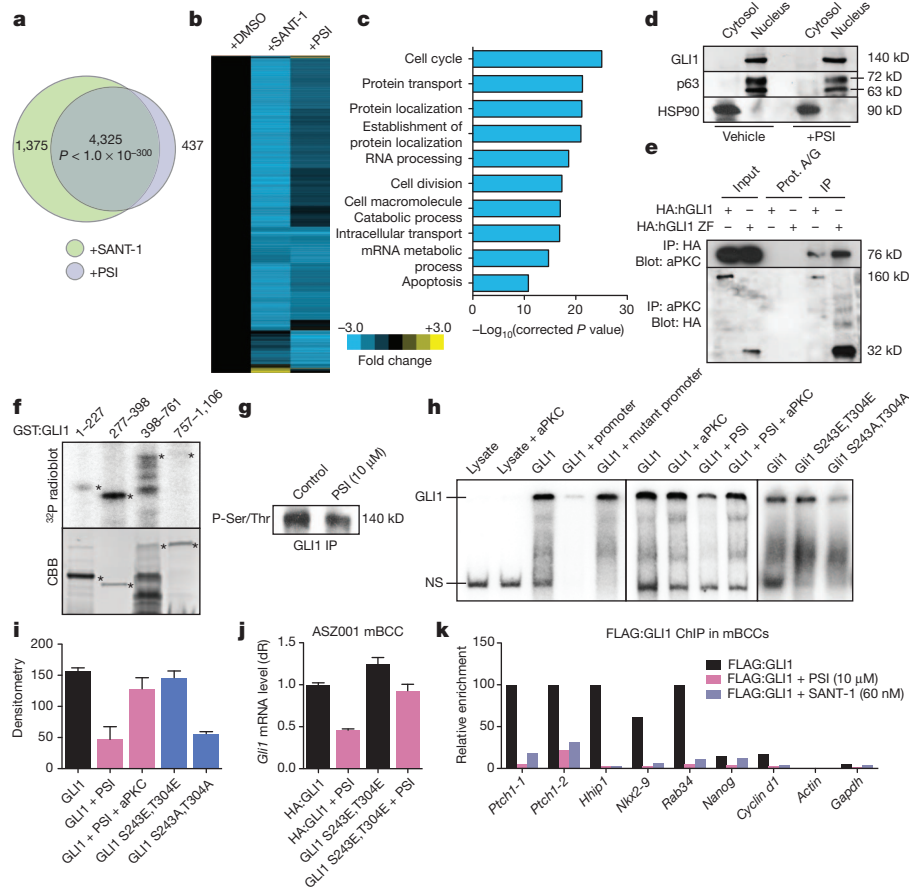


Figure 3 | aPKC-1/λ phosphorylates and activates GLI1. **a, b**, Venn diagram (**a**) and heat map (**b**) of significantly changed transcripts after SANT-1 or PSI treatment in BCC cells. **c**, Gene ontology terms of commonly altered transcripts. **d**, PSI does not affect nuclear GLI1 in BCC cells. **e**, aPKC-1/λ interacts with IVT human GLI1 or GLI1 DNA-binding domain. **f**, aPKC-1/λ phosphorylates human GLI1 DNA-binding domain. CBB, Coomassie brilliant blue. **g**, PSI reduces phosphorylated serine/threonine levels of immunoprecipitated GLI1

correlation of 0.495. Comparison with previously published HH-dependent data sets from mouse medulloblastomas/granular neural precursors or developing mouse limb bud^{15,16} reveals substantial overlap (Supplementary Fig. 4a). We found that 321 of the 1,077 GLI1-binding sites found in medulloblastomas/granular neural precursors ($P = 1.36 \times 10^{-11}$) and 41 of the 396 GLI3-binding sites identified in the developing limb bud ($P = 8.92 \times 10^{-9}$) overlap with our commonly changed data set. Representative gene expression profiles among the data sets are displayed in a cluster heat map in Supplementary Fig. 4b. Validation of a subset of transcript expression levels using quantitative reverse-transcription PCR shows that the relative values from our data set closely mirror actual mRNA levels on drug treatment (Supplementary Fig. 4c, d). These results indicate that aPKC-1/λ and SMO regulate a common set of HH target genes in BCCs.

The striking overlap of transcriptional targets suggested that aPKC-1/λ might regulate GLI transcription factors. To determine where aPKC-1/λ acts, we added subthreshold concentrations of cyclopamine or PSI to BCC cells. We found that only cyclopamine outcompeted SAG-mediated activation (Supplementary Fig. 5a), indicating that aPKC-1/λ functions downstream of SMO. Moreover, aPKC-1/λ inhibition slightly increases rather than decreases GLI1 stability (Supplementary Fig. 5b), does not affect GLI2 or GLI3 processing (Supplementary Fig. 5c), and does not alter GLI1 nuclear localization (Fig. 3d and Supplementary Fig. 5d), suggesting that aPKC-1/λ affects GLI activity. Intriguingly, loss of aPKC-1/λ protein in mouse fibroblasts results in a GLI1 band with slightly smaller apparent

molecular weight (Supplementary Fig. 5e, f). By contrast, loss of MIM, despite primary cilia defects that prevent substantial activation of the HH pathway⁸, have more aPKC-1/λ protein and a GLI1 band with a slightly larger apparent molecular weight, suggesting aPKC-1/λ modifies GLI1 post-translationally. Consistent with the notion of aPKC-1/λ-dependent alteration of GLI1 activity, aPKC-1/λ and GLI1 form a complex as recombinant HIS:aPKC-1/λ and *in vitro*-translated (IVT) human HA:GLI1 or HA:GLI1 zinc-finger co-immunoprecipitate (Fig. 3e). Purified aPKC-1/λ directly phosphorylates GLI1 *in vitro* (Fig. 3f), with the majority of the phosphorylation occurring in the zinc-finger DNA-binding region of GLI1. Immunoprecipitation of endogenous GLI1 from BCC cells shows PSI-dependent phosphorylation at serine/threonine residues, further supporting an *in vivo* role for aPKC-1/λ (Fig. 3g).

PSI-treated IVT human GLI1:V5/HIS, where endogenous aPKC-1/λ is inhibited in the reaction, significantly reduced binding to radio-labelled *GLI1* target DNA in an electrophoretic mobility assay (Fig. 3h, i). Addition of recombinant aPKC-1/λ overcame the effects of PSI to rescue GLI1-dependent DNA binding, whereas the addition of heat-inactivated aPKC-1/λ did not (Supplementary Fig. 5g), indicating that GLI1 phosphorylation by aPKC-1/λ is necessary for maximal DNA binding. The phosphorylation state of GLI1 seems to be critical because higher concentrations of aPKC-1/λ led to paradoxically decreased DNA binding (Supplementary Fig. 5g).

We performed a mutagenesis screen of the GLI1 DNA-binding domain to determine the site of aPKC-1/λ phosphorylation and

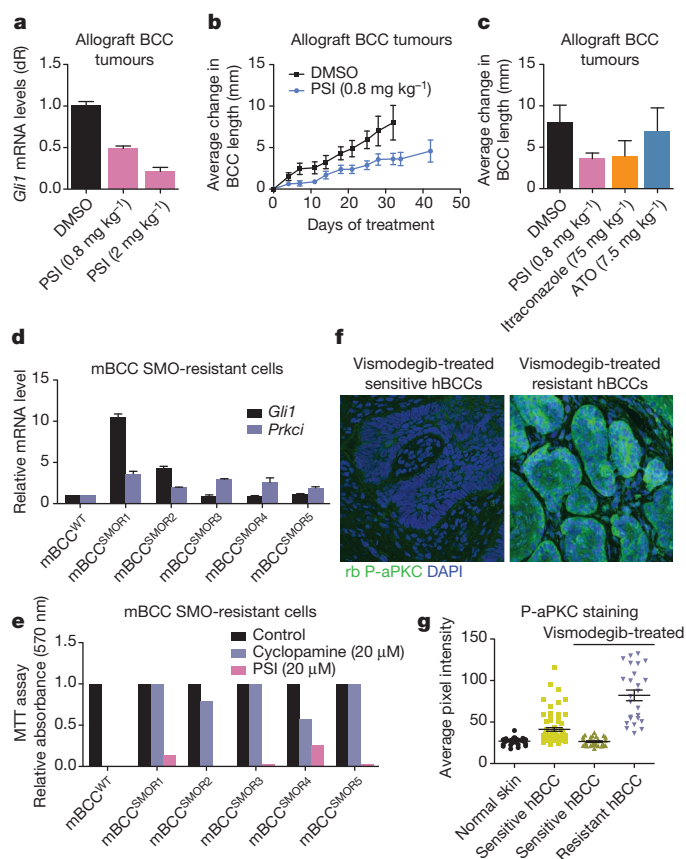


Figure 4 | Topical aPKC inhibitor suppresses primary tumour growth.

a, PSI inhibits HH signalling in allografted mouse BCC tumours from *Ptch1*^{+/-}; *K14-creER2;p53*^{lox/lox} mice ($n = 7$). **b**, Topical treatment of allografted BCC tumours slows tumour growth (DMSO, $n = 10$; PSI, $n = 9$). **c**, Intermediate levels of PSI ($n = 8$) compared with intermediate concentrations of itraconazole ($n = 8$) and arsenic trioxide ($n = 5$) after 29 days of treatment. **d, e**, Five independently derived SMO-resistant BCC cell lines (mBCC^{SMOR1} to mBCC^{SMOR5}) that amplify *Prkci* or both *Prkci* and *Gli1* mRNA levels (**d**) are sensitive to PSI treatment (**e**). mBCC^{WT}, SMO-sensitive BCC cell line. **f, g**, Vismodegib-treated resistant human BCC tumours ($n = 6$) display higher levels of active aPKC- λ than do vismodegib-treated sensitive tumours ($n = 8$), non-drug-treated tumours ($n = 17$) and normal skin ($n = 7$). Error bars, s.e.m.

found that residues Ser 243 and Thr 304 seem to mediate aPKC- λ /GLI1 effects. Phosphomimetic GLI1 (GLI1^{S243E,T304E}) bound to target DNA just as well as wild-type GLI1 did, whereas phosphodeficient GLI1 (GLI1^{S243A,T304A}), which accumulates less aPKC- λ phosphorylation (Supplementary Fig. 5h), has less DNA-binding ability (Fig. 3h, i). Moreover, GLI1^{S243E,T304E} is less sensitive to PSI in BCC cells, suggesting that these sites are functional aPKC- λ sites (Fig. 3j). To confirm that aPKC- λ regulates GLI binding *in vivo*, we performed ChIP of FLAG:GLI1 in BCC cells using GLI target genes^{17,18}. On all GLI1 targets assayed, PSI-treated tumour cells left GLI1 nuclear protein levels unchanged but reduced the association with chromatin (Fig. 3d, k). Non-HH target genes were left unchanged by PSI treatment. We conclude that aPKC- λ regulates HH signalling by phosphorylating and activating GLI1 to increase its affinity for DNA, illustrating a rare instance where post-translational modification of a zinc-finger domain promotes DNA binding and transcriptional activity.

To explore whether aPKC inhibitors can be used successfully as a BCC therapeutic, we topically treated allografted BCC tumours¹⁴ with PSI. This tumour model accurately describes human BCCs and has previously been used to validate HH pathway inhibitors now in clinical use¹⁹. In allografted BCCs, *Gli1* mRNA decreased as the concentration of topical PSI was increased (Fig. 4a). Also, tumour size was suppressed for intermediate concentrations of PSI, with no apparent acquired resistance

(Fig. 4b). This compares favourably with treatment with intermediate concentrations of SMO antagonist itraconazole¹⁹ or GLI2 inhibitor arsenic trioxide²⁰ (Fig. 4c). Tumours lost their classical palisade patterning on PSI treatment, and apoptosis increased (Supplementary Fig. 6). Cell proliferation was reduced along with GLI1 protein levels. Mice treated with topical or intraperitoneal PSI showed no apparent adverse effects (Supplementary Fig. 7) except a mild hair cycling phenotype (not shown) suggesting that aPKC treatment is tumour selective.

Because aPKC- λ acts downstream of SMO, we determined whether PSI could inhibit cell growth of SMO-resistant tumours. Following methods to generate resistant lines for other chemotherapeutics such as K-ras or B-raf²¹, we generated multiple independent BCC cell lines that were resistant to high levels of SANT-1. These SMO-resistant lines displayed increased expression of *Prkci* mRNA and protein, with varying levels of *Gli1* mRNA (Fig. 4d and Supplementary Fig. 8a). Other HH target genes displayed differential expression patterns that followed *Gli1* or *Prkci* mRNA levels, or were generally suppressed (Supplementary Fig. 8b). We verified SMO resistance by treating the cells with high concentrations of structurally unrelated cyclopamine and found little effect on cell proliferation (Fig. 4e). Treatment of these lines, or SANT-1-sensitive parental lines, with PSI drastically reduced cell proliferation, suggesting that active aPKC- λ has a role in SMO-inhibitor-resistant human tumours. Comparison of SMO-inhibitor-sensitive and SMO-inhibitor-resistant locally invasive human BCCs, several of which lacked *SMO* and *SUFU* mutations as well as *GLI1/2* amplification (B. Yauch, personal communication), showed elevated levels of active aPKC- λ in resistant tumours with polyclonal and monoclonal antibodies, corroborating the increase of active aPKC- λ levels as a mode of resistance (Fig. 4f, g and Supplementary Fig. 8c, d). Taken together, these data indicate that BCCs become dependent on aPKC- λ to drive HH activation and tumour growth, and that suppression of aPKC- λ activity is sufficient to prevent BCC progression in both SMO-sensitive and SMO-resistant lines. Our results highlight aPKC- λ inhibition as a viable, tumour-selective alternative to SMO inhibitors to treat HH-dependent and SMO-resistant cancers.

METHODS SUMMARY

All mouse studies were approved by and conformed to the policies and regulations of the Institutional Animal Care and Use Committees at Stanford University and the Children's Hospital Oakland Research Institute. *Ptch1*^{+/-}; *K14-creER2;p53*^{lox/lox} mice were used to develop BCC tumours. Tumours were allografted as previously described¹⁴. Nine tumours from three mice were treated topically twice daily with 0.8 mg kg⁻¹ PSI dissolved in DMSO for at least 32 days, with measurements on some tumours lasting 42 days. Ten tumours from three mice were treated with DMSO twice daily as a control. Mice were killed and tumours collected when tumour size exceeded the limit in our animal care guidelines. We measured the change in tumour size with callipers every three to four days. Pairwise comparisons between DMSO and PSI treatment were done using a two-sided unpaired *t*-test with GraphPad PRISM software.

The electrophoretic mobility shift assay was performed by incubation of 50 fmol double-stranded radio-labelled *GLI1* oligonucleotides (5'-AGCCCGGACCAC CCACGAGAA-3') in binding buffer (25 mM HEPES pH 7.5, 25 mM KCl, 2.5 mM MgCl₂, 1 mM DTT, 10% glycerol, 25 μ M poly(dI-dC) and 5 μ M ZnSO₄) with IVT GLI1:V5/HIS, HA:GLI1, HA:GLI1^{S243E,T304E} or HA:GLI1^{S243A,T304A} lysate for 10 min at 25 °C. Unlabelled *GLI1* oligonucleotides or *GLI1* mutant oligonucleotides (2 pmol) (5'-AGCCCGGAGGAGGCACGAGAA-3') were used as competition. Endogenous aPKC was inhibited in reticulocyte lysate with PSI during the translation reaction, and rescue was performed by adding recombinant HIS:aPKC- λ for 15 min before addition of radio-labelled *GLI1* oligonucleotides. Samples were resolved on 6% acrylamide gel, exposed to a phosphor screen (Molecular Dynamics) and imaged using a GE Typhoon 9410.

Full Methods and any associated references are available in the online version of the paper.

Received 1 May 2012; accepted 4 January 2013.

- Ng, J. M. Y. & Curran, T. The Hedgehog's tale: developing strategies for targeting cancer. *Nature Rev. Cancer* **11**, 493–501 (2011).

2. Yauch, R. L. *et al.* Smoothened mutation confers resistance to a Hedgehog pathway inhibitor in medulloblastoma. *Science* **326**, 572–574 (2009).
3. Buonamici, S. *et al.* Interfering with resistance to smoothened antagonists by inhibition of the PI3K pathway in medulloblastoma. *Sci. Transl. Med.* **2**, 51ra70 (2010).
4. Dijkgraaf, G. J. P. *et al.* Small molecule inhibition of GDC-0449 refractory smoothened mutants and downstream mechanisms of drug resistance. *Cancer Res.* **71**, 435–444 (2011).
5. Chang, A. L. S. & Oro, A. E. Initial assessment of tumor regrowth after vismodegib in advanced basal cell carcinoma. *Arch. Dermatol.* **148**, 1324–1325 (2012).
6. Atwood, S. X., Chang, A. L. S. & Oro, A. E. Hedgehog pathway inhibition and the race against tumor evolution. *J. Cell Biol.* **199**, 193–197 (2012).
7. St Johnston, D. & Ahringer, J. Cell polarity in eggs and epithelia: parallels and diversity. *Cell* **141**, 757–774 (2010).
8. Bershteyn, M., Atwood, S. X., Woo, W.-M., Li, M. & Oro, A. E. MIM and cortactin antagonism regulates ciliogenesis and hedgehog signaling. *Dev. Cell* **19**, 270–283 (2010).
9. Callahan, C. A. *et al.* MIM/BEG4, a sonic hedgehog-responsive gene that potentiates Gli-dependent transcription. *Genes Dev.* **18**, 2724–2729 (2004).
10. Aszterbaum, M. *et al.* Ultraviolet and ionizing radiation enhance the growth of BCCs and trichoblastomas in patched heterozygous knockout mice. *Nature Med.* **5**, 1285–1291 (1999).
11. Atwood, S. X. & Prehoda, K. E. aPKC phosphorylates Miranda to polarize fate determinants during neuroblast asymmetric cell division. *Curr. Biol.* **19**, 723–729 (2009).
12. Standaert, M. L. *et al.* Insulin activates protein kinases C- ζ and C- λ by an autophosphorylation-dependent mechanism and stimulates their translocation to GLUT4 vesicles and other membrane fractions in rat adipocytes. *J. Biol. Chem.* **274**, 25308–25316 (1999).
13. Winklmayr, M. *et al.* Non-consensus GLI binding sites in Hedgehog target gene regulation. *BMC Mol. Biol.* **11**, 2 (2010).
14. Wang, G. Y. *et al.* Establishment of murine basal cell carcinoma allografts: a potential model for preclinical drug testing and for molecular analysis. *J. Invest. Dermatol.* **131**, 2298–2305 (2011).
15. Lee, E. Y. *et al.* Hedgehog pathway-regulated gene networks in cerebellum development and tumorigenesis. *Proc. Natl Acad. Sci. USA* **107**, 9736–9741 (2010).
16. Vokes, S. A., Ji, H., Wong, W. H. & McMahon, A. P. A genome-scale analysis of the cis-regulatory circuitry underlying sonic hedgehog-mediated patterning of the mammalian limb. *Genes Dev.* **22**, 2651–2663 (2008).
17. Vokes, S. A. *et al.* Genomic characterization of Gli-activator targets in sonic hedgehog-mediated neural patterning. *Development* **134**, 1977–1989 (2007).
18. Po, A. *et al.* Hedgehog controls neural stem cells through p53-independent regulation of Nanog. *EMBO J.* **29**, 2646–2658 (2010).
19. Kim, J. *et al.* Itraconazole, a commonly used antifungal that inhibits Hedgehog pathway activity and cancer growth. *Cancer Cell* **17**, 388–399 (2010).
20. Kim, J., Lee, J. J., Kim, J., Gardner, D. & Beachy, P. A. Arsenic antagonizes the Hedgehog pathway by preventing ciliary accumulation and reducing stability of the Gli2 transcriptional effector. *Proc. Natl Acad. Sci. USA* **107**, 13432–13437 (2010).
21. Little, A. S. *et al.* Amplification of the driving oncogene, KRAS or BRAF, underpins acquired resistance to MEK1/2 inhibitors in colorectal cancer cells. *Sci. Signal.* **4**, ra17 (2011).

Supplementary Information is available in the online version of the paper.

Acknowledgements We would like to thank K. Qun for bioinformatics assistance, J. Kim for archival BCC tissue, A. Chang and S. Aasi for clinical trial operations, K. Chang for technical assistance, and H. Chang and P. Khavari for reading the manuscript. This work was supported by NIH NRSA 1F32CA14208701 (S.X.A.) and NIH grants AR052785 and AR046786 (A.E.O.).

Author Contributions S.X.A. and A.E.O. designed the experiments. S.X.A. performed the experiments. M.L. aided the biochemical and knockdown analyses. A.L. and J.Y.T. performed the allograft BCC drug treatments. J.Y.T. provided vismodegib-resistant tumour samples. S.X.A. and A.E.O. wrote the manuscript.

Author Information Reprints and permissions information is available at www.nature.com/reprints. The authors declare competing financial interests: details are available in the online version of the paper. Readers are welcome to comment on the online version of the paper. Correspondence and requests for materials should be addressed to A.E.O. (oro@stanford.edu) or S.X.A. (satwood@stanford.edu).

METHODS

Tumour immunofluorescence. Human tumours from SMO-inhibitor-sensitive and SMO-inhibitor-resistant patients were obtained from patients enrolled in clinical trials performed by the Stanford group (A.E.O. and J.Y.T.) and clinical trials NCT00833417 and NCT00957229. Patients gave consent under an approved Stanford IRB protocol (#18325). Active and total aPKC levels in human tumour sections were determined by immunofluorescence using rabbit anti-aPKC (1:250; Santa Cruz Biotechnology), rabbit anti-p-aPKC Thr 410 (1:100; Santa Cruz Biotechnology) or mouse anti-p-aPKC Thr 410 (1:100; Santa Cruz Biotechnology). Confocal images were acquired on a Leica SP2 AOBs laser scanning microscope with a HCX PL APO $\times 63$ oil-immersion objective. Average pixel intensity over five distinct areas per tumour section was determined using IMAGEJ. Images were arranged with IMAGEJ, Adobe PHOTOSHOP, and Adobe ILLUSTRATOR.

Cell culture. Primary mouse dermal cells were isolated as previously described⁸. Dermal cells were grown in Amniomax media containing supplement and antibiotics (Invitrogen). ASZ001 cells were grown in 154CF media containing 2% chelated FBS, HKGS supplement and antibiotics (Invitrogen). Keratinocytes (HPA Culture Collections) were grown in CnT-07 media containing supplement and 0.07 mM CaCl₂ (CellNTEc). Cells were serum-starved for between 24 and 48 h to induce ciliogenesis. The MTT cell proliferation assay was performed using the manufacturer's protocol (Invitrogen). Cells were transfected with FuGene6 or nucleofected using an Amaxa Human Keratinocyte Nucleofector kit according to the manufacturer's protocol.

SMO-resistant cell lines were generated by treating ASZ001 BCC cells with increasingly higher concentrations of SANT-1 in every passage for three weeks. Final resistant cell lines were grown in 60 μ M SANT-1. Cyclopamine was used to inhibit HH signalling to verify SMO resistance.

Antibodies and immunofluorescence staining. Cells were fixed with either 4% paraformaldehyde or 100% methanol for 10 min. Normal horse serum (1%) and 0.1% Triton X-100 in PBS was used for blocking. Tissues were fixed with 4% paraformaldehyde and embedded in paraffin. Sections (10 μ m) were cut and deparaffinized under standard conditions before staining. Tissue sections were blocked using 20% normal horse serum and 0.1% Triton X-100 in PBS. The following antibodies were used: rabbit anti-aPKC (1:500; Santa Cruz Biotechnology), rabbit anti-p-aPKC Thr 410 (1:100; Santa Cruz Biotechnology), mouse anti-p-aPKC Thr 410 (1:100; Santa Cruz Biotechnology), rabbit anti-PARD6A (1:100; Santa Cruz Biotechnology), mouse anti-PARD6A (1:100; Santa Cruz Biotechnology), mouse anti-PARD3 (1:500; Millipore), mouse anti-CDC42 (1:500; Santa Cruz Biotechnology), rabbit anti-MIM (1:1,000; ref. 8), rabbit anti- γ -tubulin (1:500; Sigma), mouse anti- γ -tubulin (1:500; Abcam), mouse anti-acetylated tubulin (1:2,000; Sigma), goat anti-GLI2 (1:500; R&D Systems), goat anti-GLI3 (1:250; R&D Systems), rat anti-HA (1:1,000; Covance), rabbit anti-KI67 (1:200; Lab Vision), mouse anti-GLI1 (1:1,000; Cell Signaling), rabbit anti-phosphoserine/threonine (1:1,000; Abcam), mouse anti-actin (1:5,000; Sigma), rabbit anti-HSP90 (1:200; Santa Cruz Biotechnology), mouse anti-p63 (1:200; Santa Cruz Biotechnology) and TUNNEL stain (Roche). Secondary antibodies were from Invitrogen. Confocal images were acquired on a Leica SP2 AOBs laser scanning microscope with a HCX PL APO $\times 63$ oil-immersion objective. Images were arranged with IMAGEJ, Adobe PHOTOSHOP, and Adobe ILLUSTRATOR.

Protein purification and binding experiments. All proteins were expressed and purified as previously described²². IVT proteins were produced using the manufacturer's protocol in rabbit reticulocyte lysate from Promega. Endogenous proteins were immunoprecipitated by using 5 μ g rabbit anti-aPKC- ι/λ , chicken anti-MIM, mouse anti-PARD3, rabbit anti-PARD6A, rat anti-HA, mouse anti-GLI1 or mouse anti-FLAG (Sigma) with protein A/G-conjugated beads according to the manufacturer's protocol (Santa Cruz Biotechnology). *In vivo*-phosphorylated GLI1 was detected by immunoprecipitation of GLI1 from BCC cells treated with 10 μ M MG132 in the presence or absence of 10 μ M PSI for 6 h. Samples were separated by SDS-polyacrylamide gel electrophoresis (PAGE) and transferred to nitrocellulose, followed by antibody incubations and visualization using chemiluminescent substrate (ThermoScientific).

Centrosomes were purified from mouse C3H 10T1/2 cells as previously described²³. Supernatant fractions were isolated by incubation of mouse BCC cells with lysis buffer (10 mM HEPES pH 7.5, 1.5 mM MgCl₂, 10 mM KCl, 0.4% NP-40) for 2 min on ice. Nuclei were spun down and washed twice with lysis buffer before equal-volume resuspension in PBS and addition of SDS loading buffer.

Kinase assays. HIS:aPKC- ι/λ (Abcam) was incubated with GST, GST:GLI1 or GST:GLI1 fragments at 30 °C for 15 min in kinase reaction buffer (20 mM Tris-HCl pH 7.5, 10 mM MgCl₂, 1 mM DTT, 10 mM ATP) with 20 nM [γ -³²P]ATP. The reaction was quenched by addition of SDS loading buffer and heated at

95 °C for 10 min. The protein was resolved by SDS-PAGE, exposed to a phosphor screen (Molecular Dynamics) and imaged using a GE Typhoon 9410.

Luciferase assays. ASZ001 cells were nucleofected (Amaxa) with pGL3-Basic (Promega) containing the following GLI-binding sites or mutant sites multimerized ($\times 6$) head to tail: site 1 (GACCCCCAA); site 1 mutant (GAAACACAG); site 2 (TGCCCCCA); site 2 mutant (TGAACACCT); site 3 (TACCCCCAAA); site 3 mutant (TAAACATAG); GLICS (GACCACCCA); GLICS mutant (GATAA TCCG). Nucleofected cells were grown to confluency and lysed, and luciferase expression was determined using the Dual-Luciferase Assay System (Promega) and a TD-20/20 Luminometer.

Lentiviral knockdown and drug treatments. Lentiviral pLKO.1 vector containing short hairpin RNAs (Open Biosystems) to *Prkci* (sh3:CCGTTCCACCATGA AATGGATA, sh5:CCAGACAGAAAGCAGGTTGTT), or pSicoR-puro vector containing shRNA to *Mtss1* (ref. 8) were used. Lentivirus containing empty vector pSicoR-puro was used for control knockdowns. Lentiviral infection was performed and cells assayed after three days for *Prkci* mRNA and four days for *Mtss1* mRNA. Protein knockdown was confirmed by western blot or qRT-PCR.

Drug treatments for cells were performed with myristoylated PSI (myr-SIYRRGARRWRKLY), myristoylated scramble peptide (myr-RGIRYRLRARSWK), SANT-1 (Tocris Bioscience), cyclopamine (Tocris Bioscience), SAG (EMD), Go6983 (Tocris Bioscience) and cyclohexamide (Sigma). Subconfluent ASZ001 cells were serum-starved and inhibitors were added for 48 h before MTT assay (Invitrogen) and for 24 h before cilia visualization and GLI target gene induction assay. Stability assays performed with ASZ001 pre-incubated with PSI for 1 h before 20 μ g ml⁻¹ cyclohexamide addition at various time points. Mouse blood parameters were tested by treating mice topically twice daily with DMSO or 0.8 mg kg⁻¹ PSI dissolved in DMSO for 3 d.

Chromatin immunoprecipitation. Protein-DNA complexes were captured by fixing ASZ001 cells expressing FLAG:GLI1 and were pre-incubated for 24 h with inhibitors, fixed for 10 min with 1% formaldehyde and quenched with 0.125 M glycine for 5 min. ChIP was performed using the manufacturer's protocol adapted from Upstate. Briefly, cells were lysed for 10 min at 4 °C in lysis buffer (50 mM HEPES pH 7.5, 140 mM NaCl, 1 mM EDTA, 10% glycerol, 0.1% NP-40, 0.2% Triton-X100, protease inhibitors (Roche) and nuclei were pelleted and lysed for 10 min at 4 °C in nuclei lysis buffer (10 mM Tris-HCl pH 8, 100 mM NaCl, 1 mM EDTA, 0.5 mM EGTA, 0.5% N-lauroylsarcosine, protease inhibitors) to obtain DNA. DNA was sheared to a range of 100–600 base pairs (bp) in size by sonication for 25 min. ChIP-grade FLAG-antibody-conjugated magnetic beads (Sigma) were incubated with nuclei lysate overnight at 4 °C. Beads were washed in RIPA buffer and DNA was reverse crosslinked by incubation at 65 °C overnight in elution buffer (50 mM Tris-HCl pH 8, 10 mM EDTA, 1% SDS). RNA and protein were digested with RNase A (0.2 μ g ml⁻¹; 37 °C for 2 h) and proteinase K (0.2 μ g ml⁻¹; 55 °C for 2 h), respectively, and DNA was purified by phenol chloroform extraction using standard protocols. Relative fold enrichment was determined by adding DNA to Brilliant II SYBR Green qPCR Master Mix Kit (Agilent Technologies) containing primers to known GLI target sites listed in Supplementary Table 1. ChIP with FLAG-antibody-conjugated magnetic beads in ASZ001 without FLAG:GLI1 was used as a negative control.

3'-end RNA sequencing. The 3'-end RNA-Seq library was generated from ASZ001 cells incubated with or without inhibitors for 24 h. RNA was purified using TRIzol (Invitrogen) and poly A-RNA selected using the micro-poly(A)purist kit (Ambion). We heat-sheared 200 ng mRNA for 12 min at 85 °C and performed first-strand cDNA synthesis using Superscript III (Invitrogen) for 1 h at 50 °C. Second-strand synthesis was performed using *Escherichia coli* DNA Ligase (Invitrogen), *E. coli* DNA Polymerase I (NEB) and *E. coli* RNase H (Epicentre) for 2 h at 16 °C. We added T4 DNA Polymerase (NEB) for an additional 15 min before quenching with EDTA. We purified double-stranded cDNA with MinElute Reaction Cleanup Kit (Qiagen). Complementary DNA was poly-A-tailed using Klenow Fragment 3' to 5' exonuclease (NEB) for 30 min at 37 °C. We ligated Illumina linker using T4 DNA Ligase (Enzymatics) overnight at 25 °C. We purified 220–300-bp bands using 3% NuSieve GTG agarose (Lonza) and a MinElute Gel Extraction Kit (Qiagen). We amplified the DNA using Phusion PCR Master Mix (NEB) and a 15-cycle PCR program. We purified 220–300-bp bands using 3% NuSieve GTG agarose (Lonza) and MinElute Gel Extraction Kit. We sequenced DNA using Illumina Genome Analyzer IIx.

We aligned 36-bp raw reads with BOWTIE using the NCBI37/mm9 reference genome. Differential expression analysis was performed on the 3' exon with the CUFFLINKS suite using mouse RefSeq gene predictions as a reference transcriptome. Annotated coding transcripts were filtered for significant expression by a RPKM of 25 in at least one sample set. Transcripts that changed by two-fold or more in drug-treated samples were hierarchically clustered using the

CLUSTER program and visualized in Java TREEVIEW. Transcripts were validated using Brilliant II SYBR Green qRT-PCR Master Mix Kit (Agilent Technologies) with primers listed in Supplementary Table 1. The two-tailed *P* value between our gene sets and other gene sets was calculated using Fisher's exact test.

22. Atwood, S. X., Chabu, C., Penkert, R. R., Doe, C. Q. & Prehoda, K. E. Cdc42 acts downstream of Bazooka to regulate neuroblast polarity through Par-6 aPKC. *J. Cell Sci.* **120**, 3200–3206 (2007).
23. Meigs, T. E. & Kaplan, D. D. Isolation of centrosomes from cultured Mammalian cells. *Cold Spring Harb. Protocols*. doi:10.1101/pdb.prot5039 (2008).